

An Average Nodal Pressure Face-based Smoothed Finite Element Method

(FS-FEM) for 3D nearly-incompressible solids

†Chen Jiang^{1,2}, G.R. Liu²

¹College of Mechanical Engineering and Vehicle Engineering, Hunan University, Changsha, China.

²Department of Aerospace Engineering and Engineering Mechanics, University of Cincinnati, USA.

*Presenting author: jc2007@hnu.edu.cn

†Corresponding author: jc2007@hnu.edu.cn

Abstract

Average Nodal Pressure (ANP) is a simple and useful technique to alleviate the volumetric locking for all element types of standard FEM, including linear 3-node Triangles (T3) and 4-node Tetrahedrons (T4). However, standard FEM using T3 and T4 elements has shown interior accuracy and convergence than FS-FEM using same elements in previous literatures. In this paper, we combine FS-FEM and ANP to propose FS-FEM/ANP using linear T4 element for nearly-incompressible solids. The proposed FS-FEM/ANP-T4 is used to calculate a benchmark, 3D Lamé problem. This 3D Lamé benchmark proves that FS-FEM/ANP-T4 is free of volumetric locking, more accurate and converging faster than FEM/ANP-T4. Meanwhile, FS-FEM/ANP-T4 still possesses the remarkable endurance of mesh distortion. Also, a rubber beam applied with pressure is calculated to verify the good stability of FS-FEM/ANP-T4 on large deformation. In addition, proposed FS-FEM/ANP-T4 is used to simulate an application, a rubber hanger loaded with exhaust gravity. Comparisons in these examples with analytical results and other methods results show FS-FEM/ANP-T4 is a better alternative of FEM/ANP-T4.

Keywords: Average Nodal Pressure, FS-FEM, Nearly-incompressible, Tetrahedron.

Introduction

Linear 3-nodes triangles (T3) and 4-nodes tetrahedrons (T4) are simplest elements for 2D and 3D problems. Because the piecewise linear shape function is used, the stress and strain are uniformly distributed within element. Consequently, Gauss integration with one Gauss point is enough. Therefore, T3 and T4 element have fastest speed. More importantly, T3 and T4 elements can be automatically generated and h-adaptive mesh refined for any geometry. On the contrary, quadrilaterals and hexahedrons can only mesh certain topology types of geometry automatically.

However, the over-stiff linear shape function of the standard FEM using T3 and T4 elements cause poor accuracy and convergence and volumetric locking issue. Therefore, linear T3 and T4 elements are not recommended by most FEM software packages. To safely use triangles and tetrahedrons for complex geometry, second-order 6-node Triangle (T6) and 10-node Tetrahedron (T10) are often suggested. But the much more Degrees Of Freedom (DOFs) of T6 and T10 than T3 and T4 cause much more memory usage and computation cost. Another approach to improve T3 and T4 element is to use the Smoothed Finite Element Method (S-FEM), based on G-space theory and weakened weak form (W2) [1]–[3].

S-FEM adopts the gradient smoothing to gain the improvement for T3 and T4 element. The gradient smoothing is a generalization of the strain smoothing technique for Element-Free

Galerkin (EFG) method [4]. Based on different gradient smoothing techniques applied to T3 and T4 element, we will have different types of S-FEMs. For 3D compressible problem with T4 element, S-FEM is classified as cell-based S-FEM (CS-FEM) [5,6], face-based S-FEM (FS-FEM) [7], node-based S-FEM (NS-FEM) [8], alpha S-FEM (α S-FEM) [9] and 3D-edge-based S-FEM (3D-ES-FEM) [10,11]. Among these variations of S-FEMs, FS-FEM and 3D-ES-FEM have been demonstrated with better accuracy and convergence than FEM. Meanwhile, all these variations of S-FEMs are spatial stable and temporal stable, except for NS-FEM which is only temporal instable. However, due to the “sufficient softness”, only NS-FEM is volumetric locking free. Hence, a selective S-FEM [12–14] is developed by combining advantages of FS-FEM or 3D-ES-FEM and NS-FEM to deal with volumetric locking of incompressible solids. The selective S-FEM is still temporal stable. Recently, some temporal stabilization techniques are also proposed for NS-FEM [15–18]. Also, a bubble enriched S-FEMs are also proposed to further alleviate pressure instability when solid has very high bulk modulus [19–21].

On the other hand, in FEM, many researchers endeavored to rectify the volumetric locking of linear T3 and T4 elements. In this paper, all these approaches are classified into six types, (1) Mixed-enhanced elements. Different approximations of displacement field and pressure field are used to yield more displacement Degrees Of Freedom (DOFs) than pressure DOFs, like MINI element enriched with “bubble function” [23] and element using Hu-Washizu three fields variational theorem [24]; (2) Pressure stabilizations. Additional stabilization term is applied to interpolated pressure field to satisfy the Babuška-Brezzi conditions, like Finite Increment Calculus (FIC) [25], Galerkin Least Square (GLS) method and direct pressure stabilization [26] and so on; (3) Composite pressure fields. Reduce the incompressible constraint by enforcing a constant pressure or strain on a patch of T3 or T4 elements, like F-bar method [27] and so on; (4) Average nodal pressure/strain. Compute the pressure or strain at nodes by averaging pressure and strain of surrounding T3 and T4 elements [22,28–30]; (5) Fractional time stepping. Calculate an intermediate displacement field using governing equation without pressure term, then use the intermediate displacement to calculate pressure at current time step and correct the intermediate displacement field to obtain displacement at current time step, like Characteristic-based Split (CBS) method [31] and fractional time stepping [32]; (6) Selective S-FEM. Like selective integration for 4-node Quadrilaterals (Q4) and 8-node Hexahedrons (H8), Selective S-FEM [12–14,33] use NS-FEM to calculate volumetric part for T3 and T4 elements.

Definitely, the most straightforward methods are definitely the Average Nodal Pressure/Strain (ANP/ANS). Meanwhile, ANP/ANS [30] can also cure the bending locking. Similar to the selective integration, the ANP/ANS can directly be used in explicit dynamic time stepping.

In this paper, the ANP is applied to alleviate volumetric locking for FS-FEM with linear T4 element. We named this method as FS-FEM/ANP-T4. Likewise, we named standard ANP as FEM/ANP-T4. Because FS-FEM/ANP inherits some merits of FS-FEM, a superior performance of FS-FEM/ANP-T4 than FEM/ANP-T4 can be expected. In addition, an Adaptive Dynamic Relaxation (ADRM) is also introduced to speed up the analysis of quasi-static process using explicit time stepping.

The rest sections of this paper are outlined as: section 2 presents the theoretical basis of FS-FEM/ANP-T4; Section 3 mainly presents the computer implementations of explicit FS-FEM/ANP-T4 and FS-FEM/ANP-T4 with ADRM; Section 4 provides examples for verification and performance test; Section 5 draws conclusions.

Theoretical Basis

In this paper, proposed FS-FEM/ANP-T4 incorporates the gradient smoothing and the average nodal pressure. The gradient smoothing brings outperforming accuracy and robustness to S-FEM. But S-FEMs are still volumetric locking except for node-based gradient smoothing. On the other hand, average nodal pressure method [29] is able to cure t volumetric locking of S-FEMs for nearly-incompressible solids.

Gradient Smoothing

Although this paper use T4 element for 3D problem, we still illustrate the gradient smoothing in two dimensional systems. The extension of 2D gradient smoothing to three dimensions is straightforward and trivial. Give a 2D domain Ω , the smoothing gradients of displacement $u_i(\mathbf{x})$ in sub-domain Ω_L of Ω are expressed as

$$\frac{\partial u_i(\mathbf{x}_L)}{\partial x_j} \approx \int_{\Omega_L} \frac{\partial u_i(\mathbf{x}_L)}{\partial x_j} \tilde{w}(\mathbf{x} - \mathbf{x}_L) d\Omega. \quad (1)$$

Use the Gauss-Green's theorem to above equation,

$$\frac{\partial u_i(\mathbf{x}_L)}{\partial x_j} \approx \int_{\partial\Omega_L} u_i(\mathbf{x}_L) \tilde{w}(\mathbf{x} - \mathbf{x}_L) \mathbf{n} d\Gamma - \int_{\Omega_L} u_i(\mathbf{x}_L) \frac{\partial \tilde{w}(\mathbf{x} - \mathbf{x}_L)}{\partial x_j} d\Omega. \quad (2)$$

where \tilde{w} is the smoothing function whose requirements will be described later, $\partial\Omega_L$ is the outer boundary of sub-domain Ω_L which is also call smoothing domain here, and \mathbf{n} is the unit outward normal of $\partial\Omega_L$, as illustrated in Figure 1.

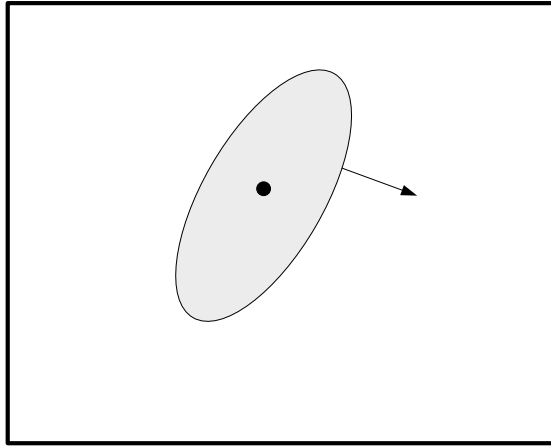


Figure 1 Generic smoothing domain.

The smoothing function in Eq.(1) can be any derivable function. Here, we adopt the suggested piecewise constant function in references [5],

$$\tilde{w} = \begin{cases} 1/A_L, & x \in \Omega_L \\ 0, & x \notin \Omega_L \end{cases} \quad (3)$$

where A_L is the area of smoothing domain.

With the piecewise constant smoothing function in Eq.(3), the second domain integral will be zero as,

$$\frac{\partial u_i(\mathbf{x}_L)}{\partial x_j} \approx \int_{\partial\Omega_L} u_i(\mathbf{x}_L) \tilde{w}(\mathbf{x} - \mathbf{x}_L) \mathbf{n} d\Gamma \quad (4)$$

As we can see, the calculation of spatial derivatives of displacements is boundary integral now and only need the displacement value. If we further discretize the displacement by FEM, the displacements can be approximated by,

$$u_i(\mathbf{x}) = \sum_{I \in G_L} \Phi(\mathbf{x}_I) u_i(\mathbf{x}_I), i = 1, 2, 3. \quad (5)$$

where $\Phi(\mathbf{x}_I)$ is the FEM shape function of node I , $u_i(\mathbf{x}_I)$ is the value of displacement at node I . G_L means supporting nodes of the smoothing domain Ω_L .

Hence, the discretized gradient of displacement is derived as,

$$\frac{\partial u_i(\mathbf{x}_I)}{\partial x_j} \approx \sum_{I \in G_L} \left(\frac{1}{A_L} \int_{\partial\Omega_L} \Phi(\mathbf{x}) n_j d\Gamma \right) u_i(\mathbf{x}_I). \quad (6)$$

where n_j is the j -th component of outward unit normal.

Compare Eq.(6) with standard calculation of gradient of displacement, the smoothed derivatives of shape functions $\bar{\Phi}_{I,j}$ are defined as,

$$\frac{\partial \bar{\Phi}_I}{\partial x_j} = \bar{\Phi}_{I,j} = \frac{1}{A_L} \int_{\partial\Omega_L} \Phi(\mathbf{x}) n_j d\Gamma. \quad (7)$$

where only shape function itself is used here, so corresponding mapping of standard FEM is no longer needed which will bring much better robustness of element distortion [6].

We have mentioned several S-FEMs for T4 element in introduction section, such as Cell-based S-FEM (CS-FEM-T4), Node-based S-FEM, Face-based S-FEM (FS-FEM-T4), Edge-based S-FEM (ES-FEM-T4) and alpha S-FEM (α S-FEM). In our previous experience, the FS-FEM-T4 is more accurate and efficient than FEM-T4. The definition of smoothing domain of FS-FEM-T4 is drawn in Figure 2(a). Also, the node-based smoothing domain of NS-FEM-T4 is also presented in Figure 2(b).

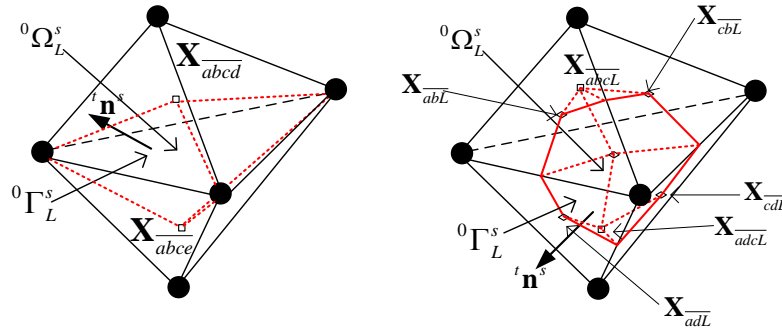


Figure 2 Smoothing domains for FS-FEM-T4 (a) and NS-FEM-T4 (b).

Average Nodal Pressure

We have already mentioned many techniques to alleviate volumetric locking to make non-locking FEM-T4 in introduction section. Among them, the average nodal pressure (ANP) is the simplest [7]–[10].

In standard ANP formulation [7], [8], the pressure is assumed as a constant within the volume associated with one node. For T4 element case, the nodal volume of node I is computed by,

$$V_I = \sum_{e=1}^{N_e} \frac{V_I^e}{4}. \quad (8)$$

where V_I is the nodal volume, N_e is the number of associated elements with node I , V_I^e is the volume of element which associate with node I .

For geometric nonlinear problems, the nodal volumetric ratio can be calculated by,

$$J_I = \frac{V_I^0}{V_I^n}. \quad (9)$$

in which, V_I^0 is the nodal volume at the initial configuration, V_I^n is the nodal volume at the current configuration.

Then, if problem is homogeneous without other materials, the ANP is given as below,

$$p_I = \kappa(J_I - 1). \quad (10)$$

where κ is the bulk modulus.

Finally, we can use this ANP to get the pressure value at the Gauss points of T4 elements. The whole process will be demonstrated more clear in later sections. In fact, the further investigation about the selective S-FEM shows the NS-FEM has some similarities with ANP to achieve volumetric locking free. The reason is that node-based gradient smoothing also gives a constant strain in node-based smoothing domain which also overlaps the same nodal volume of ANP.

Hyperelastic constitutive models

In this section, we briefly review the finite deformed hyperelasticity. Consider a solid with domain ${}^0\Omega$ at initial configuration, see Figure 3. Then after a large deformation, this solid moves and deforms to current configuration ${}^t\Omega$. The deformation is represented by the motion $\mathbf{x} = \chi(\mathbf{X}, t)$, where \mathbf{x} is the current coordinates and \mathbf{X} denotes initial or reference coordinates.

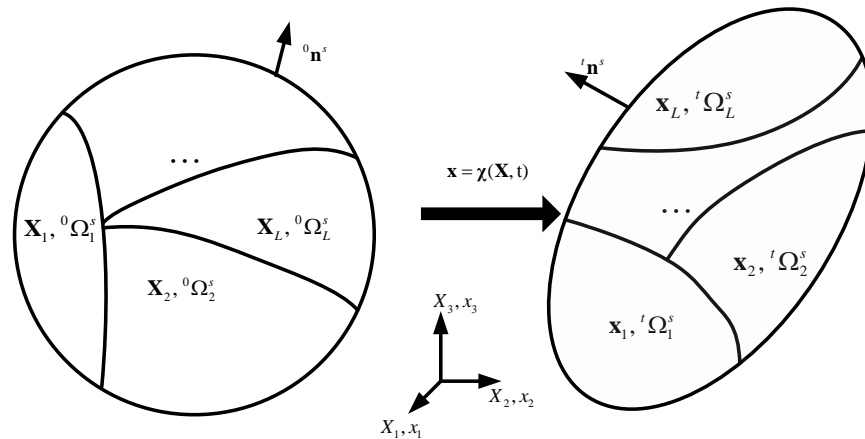


Figure 3 Configurations and deformations of a solid.

In finite deformation, the deformation gradient is important which is defined as,

$$F_{ij} = \frac{\partial x_i}{\partial X_j} + \delta_{ij} = \frac{\partial u_i}{\partial X_j} + \delta_{ij}. \quad (11)$$

After substituting smoothed strain of S-FEM, the smoothed deformation gradient is given as,

$$\bar{F}_{ij} = \sum_{l \in G_L} \bar{\Phi}_{l,j}(\mathbf{X}_L) u_{li} + \delta_{ij}. \quad (12)$$

With Eq.(12), we can get the smoothed Green strain as follows,

$$\bar{E}_{ij} = \frac{1}{2} (\bar{F}_{ki} \bar{F}_{kj} - \delta_{ij}). \quad (13)$$

Meanwhile, the smoothed right Cauchy-Green tensor $\bar{\mathbf{C}}$ is calculated as below,

$$\bar{C}_{ij} = \bar{F}_{ki} \bar{F}_{kj} \quad (14)$$

We can also get the three invariants of $\bar{\mathbf{C}}$ which are often treated as basic variables of hyperelastic material models,

$$\bar{I}_1 = \bar{C}_{ii}, \bar{I}_2 = \frac{1}{2} \left[(\bar{C}_{ii})^2 - (\bar{C}_{ij} \bar{C}_{ij}) \right], \bar{I}_3 = J^2 = \det(\bar{\mathbf{C}}). \quad (15)$$

where the third invariant \bar{I}_3 of $\bar{\mathbf{C}}$ also relates to the volumetric ratio.

The strain energy density of hyperelastic material is often decoupled into deviatoric and volumetric parts. Here the general isotropic strain energy density functions is expressed as,

$$\Psi(\bar{I}_1, \bar{I}_2, \bar{J}) = \Psi^{dev}(\bar{J}_1, \bar{J}_2) + \Psi^{vol}(\bar{J}). \quad (16)$$

where *dev* and *vol* denote the deviatoric and volumetric part of strain energy, respectively. And $\bar{J}_1 = \bar{I}_1 \bar{I}_3^{-1/3}$ is the first invariant of modified $\tilde{\mathbf{C}} = \bar{I}_3^{-2/3} \bar{\mathbf{C}}$, $\bar{J}_2 = \bar{I}_2 \bar{I}_3^{-2/3}$ is the modified second invariant of $\tilde{\mathbf{C}}$.

Although many isotropic hyperelastic strain energy density functions are proposed, the most widely used form of Ψ^{vol} is,

$$\Psi^{vol}(\bar{J}) = \frac{1}{2} \kappa (\bar{J} - 1)^2. \quad (17)$$

where κ is the bulk modulus and this part will be cared by ANP technique.

For a given hyperelastic strain energy function, the second Piola-Krichhoff (PK2) stress tensor which is also the stress measure in Total Lagrangian formulation can be calculated by FS-FEM/ANP-T4 and ES-FEM/ANP-T4,

$$\bar{\mathbf{S}} = 2 \frac{\partial \Psi^{dev}}{\partial \bar{\mathbf{C}}^{FS}} + 2 \frac{\partial \Psi^{vol}}{\partial \bar{\mathbf{C}}^{ANP}} = \bar{J}^{-2/3} \text{Dev} \tilde{\mathbf{S}} + J p^{ANP} \bar{\mathbf{C}}^{-1}. \quad (18)$$

where $\bar{\mathbf{S}}$ is the smoothed PK2 stress tensor, the *FS* is short for FS-FEM-T4, operator $\text{Dev}(\bullet) = (\bullet) - (1/3) [(\bullet) : \bar{\mathbf{C}}] \bar{\mathbf{C}}^{-1}$.

In above equation, a new fictitious PK2 stress tensor is also introduced. It can be expressed as,

$$\tilde{\mathbf{S}} = 2 \frac{\partial \Psi^{dev}(\bar{J}_1, \bar{J}_2)}{\partial \tilde{\mathbf{C}}}. \quad (19)$$

Readers can find more details about calculating the PK2 stress tensor of hyperelastic material models in reference [11].

Total Lagrangian formulations of explicit S-FEM/ANP-T4

For FEM discretization of finite deformation with Lagrangian mesh, we select the Total Lagrangian (T.L.) formulation. For temporal discretization, the explicit time integration is selected which only needs internal nodal forces.

Still consider the domain ${}^0\Omega$ in Figure 3 at reference configuration with boundary ${}^0\Gamma$. The density is ρ_0 , and a body force is applied. On the velocity boundaries ${}^t\Gamma_v$, $v_i(\mathbf{x}, t) = \hat{v}_i(\mathbf{x}, t)$. On the traction boundaries, $n_j\sigma_{ij} = h_i$ is applied. And the initial conditions are $\mathbf{v}(\mathbf{X}, 0) = \mathbf{v}_0(\mathbf{X})$ and $\mathbf{u}(\mathbf{X}, 0) = \mathbf{u}_0(\mathbf{X})$.

The energy in T.L. formulation for explicit dynamic is expressed as follow (without damping),

$$\Pi = \bar{\Pi}^{int}(\mathbf{u}) - \Pi^{ext}(\mathbf{u}) + \Pi^{kin}(\mathbf{u}), \quad \bar{\Pi}^{int} = \int_{\Omega} \Psi d\Omega. \quad (20)$$

where $\bar{\Pi}^{int}$ is the internal energy, Π^{ext} is the external energy and Π^{kin} is the kinetic energy.

In this paper, because the ANP/S-FEM is used, the strain energy is split into deviatoric and volumetric parts like below,

$$\bar{\Pi}^{int} = \bar{\Pi}^{int,dev} + \bar{\Pi}^{int,vol} \quad (21)$$

We directly give the semi-discrete equations of Eq.(20) after taking variation with smoothed Galerkin weak form [3],

$$\mathbf{M}\ddot{\mathbf{u}} = \mathbf{f}^{ext} - \bar{\mathbf{f}}^{int,dev} - \mathbf{f}^{int,vol}. \quad (22)$$

where,

$$\mathbf{M}_{IJ} = \int_{\Omega} \rho_0 [\Phi_I(\mathbf{X})]^T [\Phi_J(\mathbf{X})] d\Omega. \quad (23)$$

$$\bar{\mathbf{f}}_I^{int,dev} = \int_{\Omega} [\bar{\mathbf{B}}_I^{FS}]^T \{\bar{\mathbf{P}}^{dev}\} d\Omega = \sum_L [\bar{\mathbf{B}}_I^{FS}(\mathbf{X}_L)]^T \{\bar{\mathbf{P}}^{dev}(\mathbf{X}_L)\} {}^0A_L^s. \quad (24)$$

$$\mathbf{f}_I^{int,vol} = \int_{\Omega} [\mathbf{B}_I^{ANP}]^T \{\mathbf{P}^{ANP}\} d\Omega = \sum_L [\mathbf{B}_I^{ANP}(\mathbf{X}_L)]^T \{\mathbf{P}^{ANP}(\mathbf{X}_L)\} {}^0A_L^s. \quad (25)$$

$$\mathbf{f}_I^{ext} = \int_{\Omega} [\Phi_I(\mathbf{X})]^T \{\mathbf{b}\}_I d\Omega + \int_{\Gamma} [\Phi_I(\mathbf{X})]^T \{\mathbf{h}\}_I d\Gamma. \quad (26)$$

In above equations, \mathbf{M} can be lumped mass matrix or consistent mass matrix. $\bar{\mathbf{f}}_I^{int,dev}$ is the smoothed deviatoric internal force vector which is calculated by FS-FEM-T4. $\bar{\mathbf{f}}_I^{int,vol}$ is the volumetric internal force vector calculated by ANP method. \mathbf{P} is the first Piola-Krichhoff (PK1) stress tensor. $\bar{\mathbf{B}}_I^{FS}$ is the strain-displacement relation matrix of I -th node using FS-FEM-T4. \mathbf{B}_I^{ANP} is the strain-displacement relation matrix of I -th node using ANP which is identical to corresponding matrix of FEM-T4. More detailed equations can be found in reference [12], [13].

Then, we can use the explicit central difference scheme to implement the time integration. First, calculate the acceleration at step n using Eq.(22),

$$\mathbf{M}\ddot{\mathbf{u}}^n = \mathbf{f}^{ext}(\mathbf{u}^n, t^n) - \bar{\mathbf{f}}^{int,dev}(\mathbf{u}^n, t^n) - \mathbf{f}^{int,vol}(\mathbf{u}^n, t^n). \quad (27)$$

Then, update velocity,

$$\mathbf{v}^{n+1/2} = \mathbf{v}^{n-1/2} + \Delta t \ddot{\mathbf{u}}^n. \quad (28)$$

where Δt is the time step which is constant here.

Finally, update displacement,

$$\mathbf{u}^{n+1} = \mathbf{u}^n + \mathbf{v}^{n+1/2} \Delta t. \quad (29)$$

From the procedures of central difference scheme, it is no need to solve linear equations systems. And when lumped mass matrix is employed, the calculation of acceleration $\ddot{\mathbf{u}}$ is purely element-by-element division of two arrays which is fast and also much lesser memory usage. However, we should satisfy the conditional temporal stability of explicit central difference scheme. In the whole analysis, time step must always smaller than the critical time step which is expressed below,

$$\Delta t < \Delta t_{crit} \leq \min(l_e / c_e). \quad (30)$$

where, l_e is the characteristic length of element, c_e is sound speed of this element. The calculations of these two quantities can be found in nonlinear FEM book [14].

Adaptive Dynamic Relaxation of ANP/S-FEM

Explicit time stepping can simulate the quasi-static deformation by using a quite number of time steps. To accelerate the calculation, an adaptive dynamic relaxation (ADR) method in reference [15] are adopted by introducing the mass-scaling and mass-proportional artificial damping into governing equations. Meanwhile, the loads are divided into several load steps to apply. Furthermore, in every load step, the pseudo time stepping is used to achieve quasi-static state. The equilibrium equation at m pseudo time step in n load step is given as,

$$\mathbf{M}^{fict} \ddot{\mathbf{u}}^{n,m} = \mathbf{f}^{ext}(\mathbf{u}^n, t^n) - \bar{\mathbf{f}}^{int}(\mathbf{u}^{n,m}, t^m) - \mathbf{f}^{damping}(\mathbf{u}^{n,m}, t^m). \quad (31)$$

where \mathbf{M}^{fict} is the fictitious mass matrix by scaling from original mass matrix, $\mathbf{f}^{damping}(\mathbf{u}^{n,m}, t^m) = c_d \mathbf{M}^{fict} \mathbf{v}(t^{m-1/2})$ is the damping force with mass-proportional damping coefficient c_d , m is counter for the pseudo time step in ADR.

To check if system has reached the quasi-static state, the following criterion for displacement residual r^u is applied,

$$r^u = \left\| \mathbf{u}(t^{n+1}) - \mathbf{u}(t^n) \right\| / \left\| \mathbf{u}(t^n) \right\| < e_{adm}. \quad (32)$$

where e_{adm} is a very small positive value which is set as 10^{-6} for all cases in this study, $\|\bullet\|$ is the L2-norm.

Theoretically, \mathbf{M}^{fict} and c_d can be any values in calculation. However, there exist optimal values to achieve fastest convergence to quasi-static state. Many literatures provide massive methods to evaluate the desire \mathbf{M}^{fict} and c_d . In this paper, we select one of simplest ADR algorithm from reference [15]. This ADR only needs to scale the mass matrix to make the

critical pseudo time step always larger than 1 for every element, see Eq.(30). However, other ADRs scale the mass matrix based on the element tangent stiffness matrices [16], [17] which are not necessary for explicit dynamic FEM.

When evaluating the optimal damping coefficient c_d , this ADR is using a estimation of stiffness matrix. The calculation of optimal damping coefficient at m -th pseudo time step is given as below,

$$c_d = 2 \sqrt{\frac{[\mathbf{u}^{m+1}]^T \mathbf{K}^{esti} \mathbf{u}^{m+1}}{[\mathbf{u}^{m+1}]^T \mathbf{M}^{fict} \mathbf{u}^{m+1}}}. \quad (33)$$

where, \mathbf{K}^{esti} denotes the estimation of stiffness which is calculated as below,

$$K_{ii}^{esti} = \frac{F_{int}^m - F_{int}^{m-1}}{\Delta t \cdot v_i^{m-1/2}}. \quad (34)$$

Implementation

Flowchart of Explicit FS-FEM/ANP

I. Initialization:

- A. Set initial conditions v^0 and u^0 .
- B. $u^0 = 0, n = 0, t = 0$
- C. Compute lumped mass matrix \mathbf{M}
- D. Calculate smoothed gradient of shape functions $\bar{\Phi}_{I,i}^{FS}(\mathbf{X})$.
- E. Assemble smoothed $\tilde{\mathbf{B}}^L$ using $\bar{\Phi}_{I,i}^{FS}(\mathbf{X})$.
- F. Call subroutine *Calculate_Nodal_Force_ANP* to calculate nodal force vector $\mathbf{f}(\mathbf{u}^0, 0)$
- G. Calculate acceleration $\mathbf{a}^0 = \mathbf{M}^{-1} \mathbf{f}(\mathbf{u}^0, 0)$.

II. Temporal loop, $n = 1: n_{max}$

- A. $t^{n+1} = t^n + \Delta t^{n+1/2}, t^{n+1/2} = 1/2(t^n + t^{n+1})$.
- B. $\mathbf{v}^{n+1/2} = \mathbf{v}^n + \Delta t^{n+1/2} \mathbf{a}^n$.
- C. Impose velocity boundary conditions.
- D. $\mathbf{u}^{n+1} = \mathbf{u}^n + \Delta t^{n+1/2} \mathbf{v}^{n+1/2}$.
- E. Call subroutine *Calculate_Nodal_Force_ANP* to calculate nodal force vector $\mathbf{f}(\mathbf{u}^{n+1}, t^{n+1})$.
- F. Calculate acceleration $\mathbf{a}^{n+1} = \mathbf{M}^{-1} \mathbf{f}(\mathbf{u}^{n+1}, t^{n+1})$.
- G. $\mathbf{v}^{n+1} = \mathbf{v}^{n+1/2} + (t^{n+1} - t^{n+1/2}) \mathbf{a}^{n+1}$.
- H. Update the time step counter $n+1 \rightarrow n, \mathbf{v}^{n+1} \rightarrow \mathbf{v}^n, \mathbf{u}^{n+1} \rightarrow \mathbf{u}^n, \mathbf{a}^{n+1} \rightarrow \mathbf{a}^n$.

Flowchart of FS-FEM/ANP with ADRM

I. Initialization:

- A. Set initial conditions v^0 and u^0 .

- B. $u^0 = 0, n = 0, t = 0$
 - C. Compute lumped mass matrix \mathbf{M} .
 - D. Calculate smoothed gradient of shape functions $\bar{\Phi}_{I,i}^{FS}(\mathbf{X})$.
 - E. Assemble smoothed $\tilde{\mathbf{B}}^L$ using $\bar{\Phi}_{I,i}^{FS}(\mathbf{X})$.
 - F. Calculate original nodal volume V_a^0 for each node.
 - G. Call subroutine *Calculate_Nodal_Force_ANP* to calculate nodal force vector $\mathbf{f}(\mathbf{u}^0, 0)$
 - H. Change the density to make critical time step of every element as $\Delta t_{critical} = 1.05$.
 - I. Calculate acceleration $\mathbf{a}^0 = \mathbf{M}^{-1}\mathbf{f}(\mathbf{u}^0, 0)$.
- II. Load step loop, $nLS = 1 : nLS_max$
- A. Calculate external nodal force \mathbf{f}_{nLS}^{ext} at current load step.
 - B. Check critical time step, if $\min(\Delta t_{critical}) < 1.001$, change density to retain $\Delta t_{critical} = 1.05$; else, continue.
 - C. Pseudo temporal loop, $pn = 1 : pn_max$
 1. $t^{pn+1} = t^{pn} + \Delta t^{pn+1/2}, t^{pn+1/2} = 1/2(t^{pn} + t^{pn+1})$.
 2. $\mathbf{v}^{pn+1/2} = \mathbf{v}^{pn} + \Delta t^{pn+1/2}\mathbf{a}^{pn+1/2}$.
 3. Impose velocity boundary conditions.
 4. $\mathbf{u}^{pn+1} = \mathbf{u}^{pn} + \Delta t^{pn+1/2}\mathbf{v}^{pn+1/2}$.
 5. Call subroutine *Calculate_Nodal_Force_ANP* to calculate internal nodal force vector $\mathbf{f}^{int}(\mathbf{u}^{pn+1}, t^{pn+1})$.
 6. Calculate optimal damping coefficient c_d using Eq.(33) and Eq.(34).
 7. Calculate the damping nodal force $\mathbf{f}^{damping}(\mathbf{v}^{pn+1/2}, t^{pn+1/2}) = c_d\mathbf{M}\mathbf{v}^{pn+1/2}$.
 8. Calculate acceleration $\mathbf{a}^{pn+1} = \mathbf{M}^{-1}(\mathbf{f}^{ext} - \mathbf{f}^{damping} - \mathbf{f}^{int})$.
 9. $\mathbf{v}^{pn+1} = \mathbf{v}^{pn+1/2} + (t^{pn+1} - t^{pn+1/2})\mathbf{a}^{pn+1}$.
 10. Update pseudo-time step counter $pn+1 \rightarrow pn$, $\mathbf{v}^{pn+1} \rightarrow \mathbf{v}^{pn}$, $\mathbf{u}^{pn+1} \rightarrow \mathbf{u}^{pn}$, $\mathbf{a}^{pn+1} \rightarrow \mathbf{a}^{pn}$.
 11. Check displacement residual, if $r_d < e_{adm}$, back to step C; else, continue pseudo temporal loop.

Flowchart of Subroutine Calculate_Nodal_Force_ANP in S-FEM (SD-by-SD)

Deviatoric part:

- I. **For each SD:** calculate smoothed deformation gradient $\tilde{\mathbf{F}}_{SD}^{n+1}$.
- II. **For each SD:** Calculate smoothed right Cauchy-Green strain tensor $\tilde{\mathbf{C}}^{n+1}$.
- III. **For each SD:** Calculate the invariants $\tilde{I}_i (i=1,2,3)$ of smoothed right Cauchy-Green strain tensor $\tilde{\mathbf{C}}^{n+1}$.
- IV. **For each SD:** Calculate smoothed PK2 stress $\tilde{\mathbf{S}}^{n+1}$ using selected hyperelastic strain energy density function.
- V. **For each SD:** Calculate $\tilde{\mathbf{B}} = \tilde{\mathbf{B}}^L + \tilde{\mathbf{B}}^{NL}(\mathbf{u}^{n+1}, t^{n+1})$.

VI. **For each node:** Calculate smoothed deviatoric internal force vector $\tilde{\mathbf{f}}_{dev}^{int}(u^{n+1}, t^{n+1})$.

Volumetric part:

I. **For each element:** Calculate volume V_e .

II. **For each node:** Calculate nodal volume $V_a = V_e + V_e / 4$.

III. **For each node:** Calculate nodal pressure $p_a = \kappa(J_a - 1) = \kappa(V_a / V_a^0 - 1)$.

IV. **For each element:** Calculate element's pressure $p_e = \frac{1}{n} \sum_{a=1}^4 p_a$.

V. **For each element:** Calculate volumetric PK2 stress $\tilde{\mathbf{S}}^{n+1}$, and $\tilde{\mathbf{B}} = \tilde{\mathbf{B}}^L + \tilde{\mathbf{B}}^{NL}(u^{n+1}, t^{n+1})$.

VI. **For each node:** Calculate smoothed volumetric internal force vector $\tilde{\mathbf{f}}_{vol}^{int}(u^{n+1}, t^{n+1})$.

VII. **For each node:** Calculate external force vector $\mathbf{f}^{ext}(t^{n+1})$.

VIII. **For each node:** Calculate $\mathbf{f}(u^{n+1}, t^{n+1}) = \mathbf{f}^{ext}(t^{n+1}) - \tilde{\mathbf{f}}_{dev}^{int}(u^{n+1}, t^{n+1}) - \tilde{\mathbf{f}}_{vol}^{int}(u^{n+1}, t^{n+1})$.

Numerical Examples

3D Lamé problem

The 3D Lamé problem, a 1/8 sphere inflated with internal pressure, is widely used to validate and benchmark numerical methods for 3D solid mechanics. The accuracy and convergence of proposed FS-FEM/ANP with ADRM are tested by comparing with analytical solution. The inner radius $a = 1m$ and outer radius $b = 2m$. The internal pressure applied is $P = 1pa$. This small internal pressure applied here is to coincide with analytical solution from small deformation theory. The mesh of this 3D Lamé problem with 2553 nodes is presented in Figure 4. The surfaces on the symmetry planes are all imposed with symmetrical boundary conditions. The material model in this example is the nearly-incompressible Neo-Hookean hyperelastic model with following strain energy density function,

$$\Psi(\bar{I}_1, \bar{I}_2, \bar{J}) = \Psi^{dev}(\bar{J}_1, \bar{J}_2) + \Psi^{vol}(\bar{J}) = C_{10}(\bar{J}_1 - 3) + \frac{1}{2}\kappa(\bar{J} - 1)^2. \quad (35)$$

where $C_{10} = 500pa$, the value of κ is calculated by user-defined Poisson's ratio ν as below,

$$\kappa = \frac{4(1+\nu)}{3(1+2\nu)} C_{10}.$$

The analytical solution of 3D Lamé problem with Neo-Hookean material is available in spherical coordinate system as below,

$$\begin{cases} u_r = \frac{Pa^3 r}{4C_{10}(1+\nu)(b^3 - a^3)} \left[(1-2\nu) + (1+\nu) \frac{b^3}{2r^3} \right], \\ \sigma_r = \frac{Pa^3(b^3 - r^3)}{r^3(a^3 - b^3)}, \\ \sigma_\theta = \frac{Pa^3(b^3 + 2r^3)}{2r^3(b^3 - a^3)}. \end{cases} \quad (36)$$

Validation

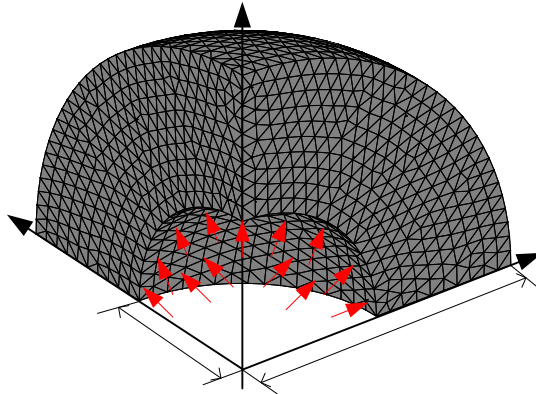


Figure 4 3D Lame configuration and mesh with 2553 nodes.

As a validation, proposed FS-FEM/ANP-T4 with the ADRM is used to solve the 3D Lame problem with Poisson's ratio 0.49. Two load steps are used for methods using ADRM. The steady state of each load step is reached when displacement residual is smaller than $1e-6$. The radial displacement, radial and tangential stresses on $x \in (0.0, 1.0)$ of FS-FEM/ANP-T4 are compared with analytical solution. Besides, displacement and stress solutions of FS/NS-FEM-T4 with ADRM, FS/NS-FEM-T4 with static solver, FEM/ANP-T4 with DRM and FEM-T4 with static solver are also compared in Figure 5 and Figure 6.

FEM-T4 has the worst displacement and stresses accuracies. Besides, the radial and tangential stresses on $x \in (0.0, 1.0)$, S_{11} and S_{33} are components of pressure. Therefore, the oscillations of S_{11} and S_{33} are just the pressure check-board issue. On the other hand, methods with ANP and NS-FEM to deal with volumetric deformation show much better performances than FEM-T4 on accuracy and stability of pressure.

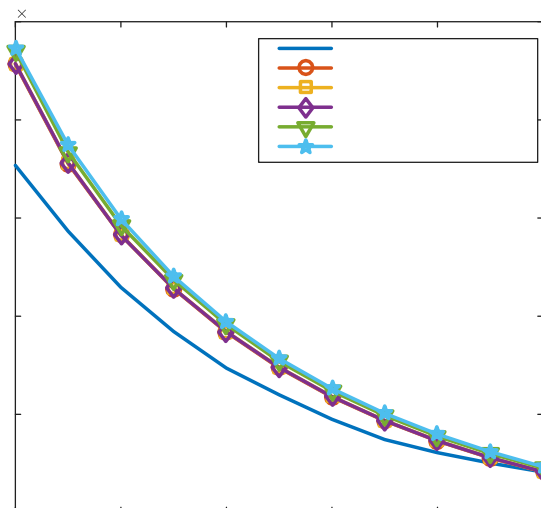


Figure 5 The radial displacements on line $x = (0.0, 1.0)$ of different methods.

To further quantify the oscillation level of these methods, the absolute S33 errors on each node of line $x \in (0.0, 1.0)$ are plotted in Figure 7. Proposed FS-FEM/ANP has smoother changes of S33 than the rest with averaged absolute errors as 0.02773. The averaged absolute errors are 0.03701 for FEM/ANP and 0.0458 for FS/NS-FEM. Hence, our implementation of FS-FEM/ANP with ADRM is correct and ANP can obtain smoother pressure distribution than NS-FEM.

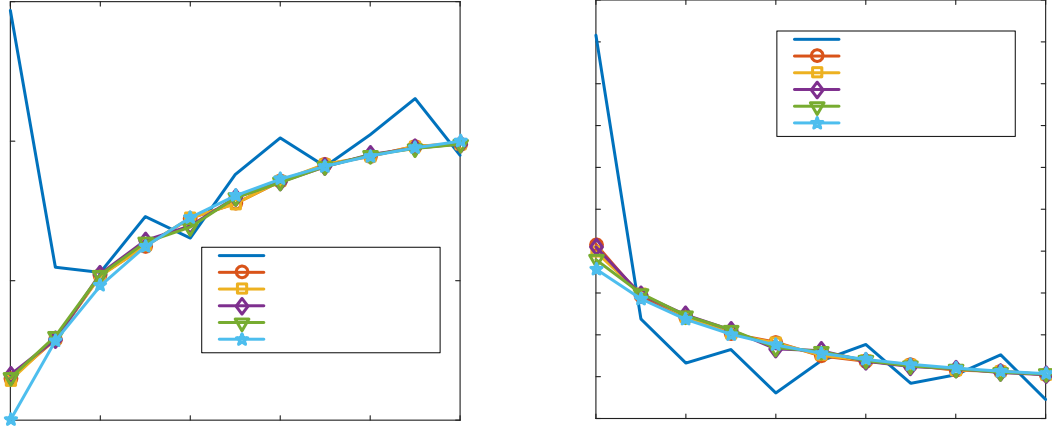


Figure 6 The radial stress σ_{xx} (a) and tangential stress σ_{zz} (b) on line $x = (0.0, 1.0)$ of different methods.

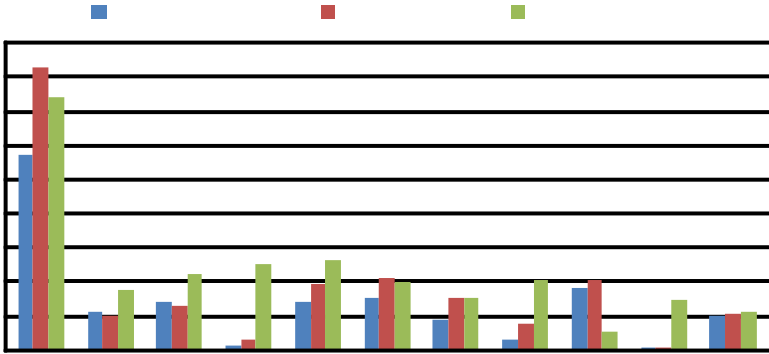


Figure 7 Absolute errors of σ_{zz} on line $x = (0.0, 1.0)$ of different methods, and average absolute errors of different methods are 0.02773 (FS-FEM/ANP), 0.03701 (FEM/ANP), and 0.0458 (FS/NS-FEM).

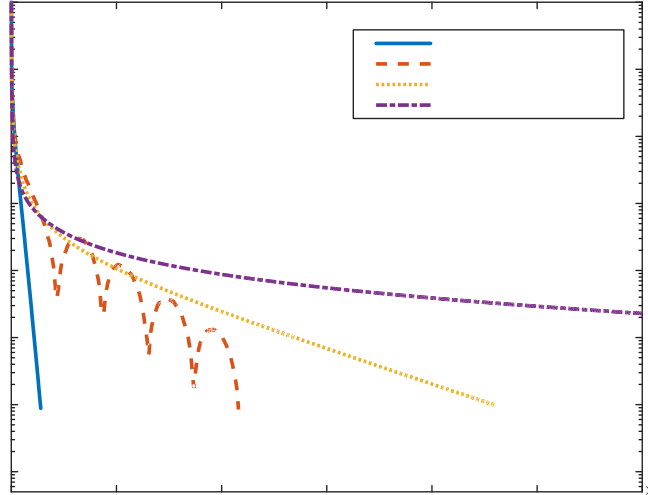


Figure 8 The displacement residual histories of Adaptive Dynamic Relaxation (ADRM) and Conventional Explicit Dynamic Relaxation (CEDRM) using FS-FEM/ANP-T4.

We also tested presented ADRM using this 3D Lamé problem. As mentioned before, three load steps are used here to gradually apply the external pressure loading. The Conventional Explicit Dynamic Relaxation (CEDRM) with different damping coefficients is also adopted as comparisons. The number of pseudo time steps of the first load step to reach the steady state is used as indicator of the performance of ADRM and CEDRM. The residual histories of different DRMs are plotted in Figure 8. CEDRMs with damping coefficient 10.0 and 100.0 are with over damping effects; the latter can't satisfy the criterion even after 100,000 pseudo time steps. CEDRM with damping coefficient 1.0 reaches steady state much faster despite of the under damping effect. As supposed, ADRM can straightly reach steady state without need to tune damping coefficient.

As Average Nodal Pressure (ANP) technique has been incorporated into FS-FEM, first time for S-FEM family, its endurance of volumetric locking is also tested, see [错误!未找到引用源。](#) and Figure 9. Here, the L2-norm of relative radial displacement is used to indicate the accuracy,

$$e_d = \sqrt{\sum_{i=1}^{N_n} (\mathbf{u}_i^{exact} - \mathbf{u}_i^{numerical})^2} / \sqrt{\sum_{i=1}^{N_n} (\mathbf{u}_i^{exact})^2}. \quad (37)$$

where \mathbf{u}_i^{exact} is analytical displacement, $\mathbf{u}_i^{numerical}$ is the displacement obtained by given numerical methods.

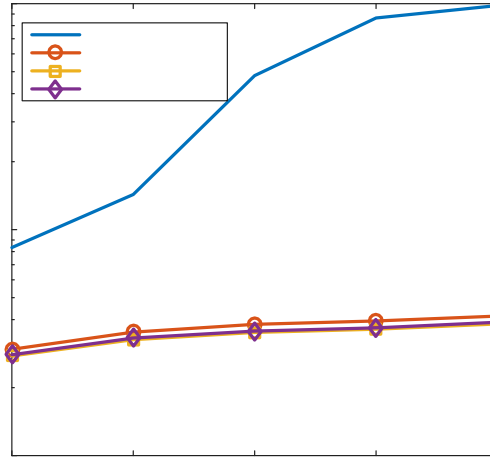


Figure 9 Volumetric locking test for FS-FEM-T4, FEM/ANP-T4, FS-FEM/ANP-T4 and FS/NS-FEM-T4.

Although the errors all tested methods are increasing when Poisson's ratio increasing, they are still under control and less than 5% for all chosen Poisson's ratios except for FS-FEM-T4. With ANP or NS-FEM, FS-FEM suffers a high volumetric locking with increasing Poisson's ratio. Another observation is that both FS-FEM/ANP and FS/NS-FEM has higher accuracies than FEM-ANP. It may be caused by the higher accuracy of FS-FEM for the deviatoric deformation. In fact, there lacks of such volumetric locking endurance test for ANP in previous literatures [7], [18].

Table 1. Volumetric locking test: the radial displacement L2-norm ed of different methods versus several Poisson's ratios.

Poisson's ratio	FS-FEM/ANP	FEM/ANP	FS/NS-FEM	FS-FEM
0.4	0.0276	0.0296	0.0280	0.08337
0.49	0.0326	0.0352	0.0331	0.14307
0.499	0.0351	0.0381	0.0356	0.48062
0.4999	0.0363	0.0394	0.0368	0.86474
0.49999	0.0386	0.0414	0.0389	0.98159

The convergences of displacement and strain energy of FS-FEM/ANP are also studied and compared with convergences of FEM/ANP and FS/NS-FEM. Here, the relations between number of nodes and radial displacement L2-norm error of tested methods are plotted in Figure 10(a). In Figure 10(a), all three methods can converge to analytical solution. Among them, FS-FEM/ANP and FS/NS-FEM get the almost identical convergence curves. This means that ANP has almost same performance to NS-FEM when selectively used for volumetric deformation. In addition, FS-FEM/ANP can always get smaller displacement error than FEM/ANP on all meshes. This comparison proves the higher displacement accuracy of FS-FEM than FEM again. In Figure 10(b), strain energy convergence curves of three methods show same features of previous displacement convergence curves.

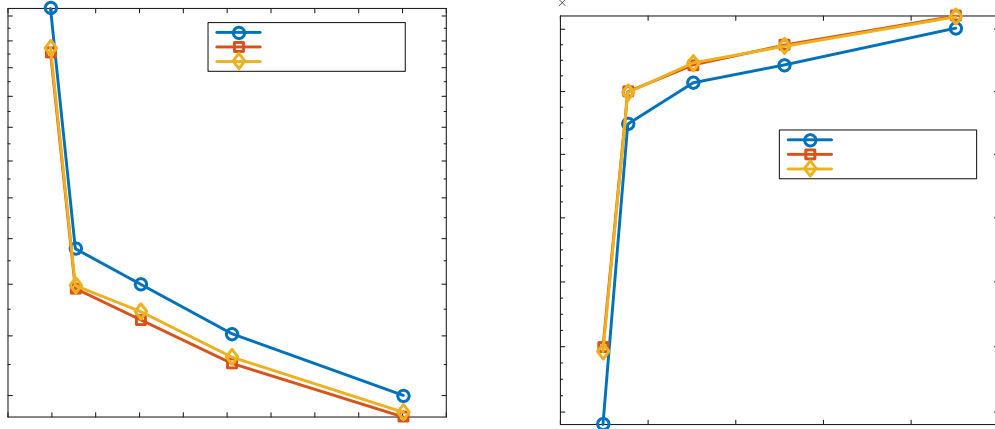


Figure 10 The radial displacement and strain energy convergences of FS-FEM/ANP, FEM/ANP and FS/NS-FEM.

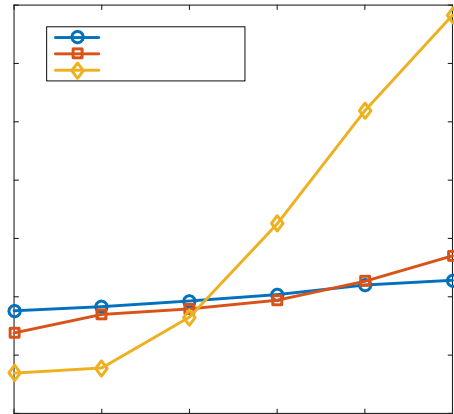
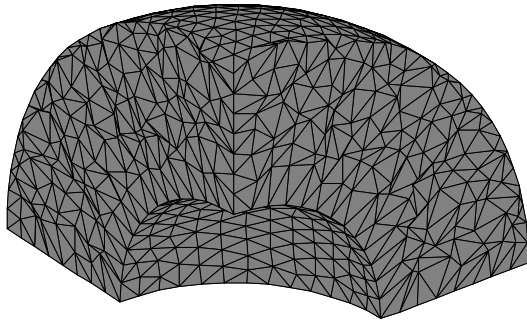


Figure 11 (a) The distorted mesh with distortion coefficient 0.5, (b) Radial displacement errors versus the distortion coefficient.

Another extraordinary capability of S-FEM family is the remarkable mesh distortion robustness. Previous studies have shown tiny accuracy deterioration even when some elements are collapsed [12], [19]. For the first time of S-FEM family embracing ANP, the evaluation of FS-FEM/ANP mesh distortion robustness is necessary. Like previous works, the artificial distortion of mesh is conducted by updating node coordinates of the non-distorted mesh with following equation,

$$\begin{cases} x' = x + h \cdot r_c \cdot \alpha \\ y' = y + h \cdot r_c \cdot \alpha \\ z' = z + h \cdot r_c \cdot \alpha \end{cases} \quad (38)$$

where α is the distortion coefficient from 0 to 1, h is the characteristic length of initial element. r_c is a random number between -1 to 1.

As a further development upon FEM/ANP, we also evaluate the mesh distortion robustness of FEM-ANP with T4 element which is also never evaluated before. After cure the volumetric locking of FEM-T4 with ANP, we can expect the similar mesh distortion robustness of FEM/ANP-T4 to FS-FEM/ANP-T4 for nearly-incompressible solids. This expectation is based on the fact that FEM-T4 is just a special case of Cell-Based S-FEM (CS-FEM) for T4 element [5]. In Figure 11 (a), one mesh of 3D Lane problem with distortion coefficient 0.5 is presented. We can see several elements are severe distorted. Then, to be a more comprehensive comparison, the mesh distortion robustness of FEM-T10 with Selective Reduced Integration (FEM/SRI-T10) is also evaluated. The relation between distortion coefficient and radial displacement L2-norm error of all evaluated methods is plotted in Figure 11(b). When mesh quality is good, the second-order FEM/SRI-T10 has smallest displacement error, then FS-FEM/ANP-T4 and FEM/ANP-T4. However, the increasing distortion coefficients aggravate the error of FEM/SRI-T10 much faster than FS-FEM/ANP-T4 and FEM/ANP-T4. Therefore, we conclude that ANP has no influence on extraordinary mesh distortion robustness of S-FEM. By the way, due to random element distortion, the mesh with distortion coefficient 0.5 for FS-FEM/ANP-T4 may locally more severe than the mesh with distortion coefficient 0.5 for FEM/ANP-T4. Therefore, the error of FS-FEM/ANP-T4 may be slightly larger than FEM/ANP-T4. In summary, researchers should pay meticulous attention to mesh quality when using FEM/SRI-T10.

Conclusions

In this paper, the FS-FEM/ANP-T4 has been proposed to solve 3D explicit dynamic and quasi-static problems of nearly-incompressible solids. In FS-FEM/ANP-T4, the FS-FEM is used for deviatoric deformation. And the ANP responds to the volumetric deformation. Several features of FS-FEM/ANP-T4 have been confirmed by selected numerical examples.

The ANP can provide the “under integration” effects to FS-FEM which is ideal for volumetric part deformation of nearly-incompressible solids.

Although FS-FEM/ANP-T4 still encounters pressure oscillation issue, it shows more mild pressure oscillation than FEM/ANP-T4 and FS/NS-FEM-T4.

FS-FEM/ANP-T4 has higher accuracy and convergence than FEM/ANP-T4. The “overly-stiff” behavior of linear T4 element is relieved by FS-FEM. FS-FEM can improve the performance for the deviatoric part deformation of nearly-incompressible solids.

FS-FEM/ANP-T4 is still very robust for mesh distortion as FS-FEM-T4. Because the ANP is based on FEM-T4 which is also special case of CS-FEM-T4.

Since the ANP is not too “soft”, FS-FEM/ANP-T4 also works well for large deformation of nearly-incompressible solids.

FS-FEM/ANP-T4 use much less computational time than FEM/RI-T10 with same mesh in explicit dynamic simulation.

Acknowledgement

The first author is partially supported by the scholarship No.201406130010 of China Scholarship Council and the National Natural Science Foundation of China under grant No. 11372106 and No. 11202075. This theoretical basic research by the senior author is partially sponsored by NSF under the Award No. DMS-1214188 and the National Natural Science Foundation of China (Grant No. 11472184). The authors would like to thank the valuable supports leading to this paper.

References

- [1] G. R. LIU, "ON G SPACE THEORY," *Int. J. Comput. Methods*, vol. 06, no. 02, pp. 257–289, 2009.
- [2] G. R. Liu, "A G space theory and a weakened weak (W₂) form for a unified formulation of compatible and incompatible methods: Part I theory," *Int. J. Numer. Methods Eng.*, vol. 81, no. 9, pp. 1093–1126, 2010.
- [3] G. R. Liu and G. Y. Zhang, *The Smoothed Point Interpolation Methods – G Space Theory and Weakened Weak Forms*. WorldScientific, 2013.
- [4] J. Chen, C. Wu, S. Yoon, and Y. You, "A stabilized conforming nodal integration for Galerkin mesh-free methods," *Int. J. Numer. Methods Eng.*, vol. 50, no. February 2000, pp. 435–466, 2001.
- [5] G. R. Liu and N. T. Trung, *Smoothed Finite Element Methods*. Boca Raton: CRC Press, 2010.
- [6] G. R. Liu, K. Y. Dai, and T. T. Nguyen, "A Smoothed Finite Element Method for Mechanics Problems," *Comput. Mech.*, vol. 39, no. 6, pp. 859–877, May 2006.
- [7] J. Bonet and A. J. Burton, "A simple average nodal pressure tetrahedral element for incompressible and nearly incompressible dynamic explicit applications," *Commun. Numer. Methods Eng.*, vol. 14, no. 5, pp. 437–449, May 1998.
- [8] J. Bonet, H. Marriott, and O. Hassan, "An averaged nodal deformation gradient linear tetrahedral element for large strain explicit dynamic applications," *Commun. Numer. Methods Eng.*, vol. 17, no. 8, pp. 551–561, Jul. 2001.
- [9] G. R. Joldes, A. Wittek, and K. Miller, "Non-locking tetrahedral finite element for surgical simulation," *Commun. Numer. Methods Eng.*, vol. 25, no. September 2008, pp. 827–836, 2009.
- [10] C. R. Dohrmann, M. W. Heinstein, J. Jung, S. W. Key, and W. R. Witkowski, "Node-based uniform strain elements for three-node triangular and four-node tetrahedral meshes," *Int. J. Numer. Methods Eng.*, vol. 47, no. June 1999, pp. 1549–1568, 2000.
- [11] G. Holzapfel, "Nonlinear Solid Mechanics: A Continuum Approach for Engineering," 2000.
- [12] C. Jiang, Z.-Q. Zhang, G. R. Liu, X. Han, and W. Zeng, "An edge-based/node-based selective smoothed finite element method using tetrahedrons for cardiovascular tissues," *Eng. Anal. Bound. Elem.*, vol. 59, pp. 62–77, 2015.
- [13] C. Jiang, Z.-Q. Zhang, X. Han, and G. R. Liu, "Selective smoothed finite element methods for extremely large deformation of anisotropic incompressible bio-tissues," *Int. J. Numer. Methods Eng.*, pp. 1–39.
- [14] T. Belytschko, W. . Liu, and B. Moran, *Nonlinear Finite Elements for Continua and Structures*. Hoboken, NJ: John Wiley & Sons, 2013.
- [15] R. G. Sauvé and D. R. Metzger, "Advances in Dynamic Relaxation Techniques for Nonlinear Finite Element Analysis," *J. Press. Vessel Technol.*, vol. 117, no. 2, p. 170, 1995.
- [16] D. R. Oakley and N. F. Knight, "Adaptive dynamic relaxation algorithm for non-linear hyperelastic structures Part II. Single-processor implementation," *Comput. Methods Appl. Mech. Eng.*, vol. 126, no. 1–2, pp. 91–109, Sep. 1995.
- [17] R. Oakley and F. Knight, "Adaptive Dynamic Relaxation algorithm for non-linear hyperelastic structures Part I. Formulation," *Comput. Methods Appl. Mech. Eng.*, vol. 25, no. 95, pp. 67–89, 1993.
- [18] J. Bonet, H. Marriott, and O. Hassan, "An averaged nodal deformation gradient linear tetrahedral element for large strain explicit dynamic applications," *Commun. Numer. Methods Eng.*, vol. 17, no. 8, pp. 551–561, Jul. 2001.
- [19] C. Jiang, G.-R. Liu, X. Han, Z.-Q. Zhang, and W. Zeng, "A Smoothed finite element method for analysis of anisotropic large deformation of passive rabbit ventricles in diastole," *Int. j. numer. method. biomed. eng.*, vol. 31, 2015.